Open Access Journal

Journal of Power Technologies 97 (5) (2017) 373–381

journal homepage:papers.itc.pw.edu.pl

Thermal-FSI modeling of flow and heat transfer in a heat exchanger based on minichanels

Sebastian Kornet[a,*], Paweł Ziółkowski[a], Paweł Jóźwik[b], Piotr Józef Ziółkowski[a,c], Michał Stajnke[a], Janusz Badur[a]

[a] *Energy Conversion Department, Institute of Fluid Flow Machinery, Polish Academy of Sciences, Fiszera 14, 80-231 Gdańsk, Poland;*
[b] *Department of Advanced Materials and Technologies, Faculty of Advanced Technologies and Chemistry, Military University of Technology, Kaliskiego 2 Str., 00-908 Warszawa, Poland;*
[c] *Department of Mechanics of Materials and Structures, Faculty of Civil and Environmental Engineering, Gdańsk University of Technology, Narutowicza 11/12,80-233 Gdańsk, Poland*

Abstract

In this paper selected numerical modelling problems for an advanced thermal-FSI ("Fluid Solid Interaction") mini-channel heat exchanger model are presented. Special attention is given to the heat transfer between the separated mediums for different mass flows. Similar modelling problems have also been discussed in the literature dedicated to numerical and theoretical modelling problems for typical heat exchangers [1, 2, 3]. Basic tests, including a comparison with experimental data, have been conducted using a Mini-channel Plate Heat Exchanger (MPHE). The MPHE was made out of two gasketed brazed plates with 40 mm long rectangular cross section channels (width—1 mm, depth—700 μm).The thermal-FSI analysis was applied for the heat exchanger model with one hot and one cold water flow passage through the mini-channels. Satisfactory agreement between the modelling results and the experimental data [4] was obtained.

Keywords: CFD modelling; Mini-channel; Heat exchanger; Heat transfer; Thermal-FSI

1. Introduction

High temperatures induce thermal stress and are present in many engineering applications and analyses. Therefore, heat transfer and thermal management are very important design parameter for many products. Failure to control heat can lead to major safety and efficiency problems. Thermal management mostly includes: material deformation and stress from heat, the efficient removal of heat, the impact of thermal cycling on the durability of the device, appropriate heating for the activation of thermocatalytic reactions, and the desired operation of heat exchangers [1, 2, 3]. In recent years, heat exchanger manufacturer focused on the reduction of the products size and weight as well as on ways to reduce costs of production, increase reliability, boost the efficiency of heat transfer, increase lifecycle, and meet energy efficiency and emission requirements of contemporary stringent standards [4, 5, 6, 7, 8, 9, 10, 11].

A high heat transfer rate using minimum pumping power and space are very important aspects in current heat exchanger design strategies [9, 10, 11, 12, 13, 14, 15]. When low thermal conductivity fluids are used in the heat exchanger, there is a need to increases the heat transfer rate. One way to improve the heat transfer rate with low conductivity fluids is to introduce a disturbance in the fluid flow, but this solution can lead to a significantly increase in pumping power followed by unacceptably high system costs [14, 15, 16, 17, 18]. Therefore, other techniques are used to achieve the desired heat transfer rate at an economical pumping power [18, 19, 20, 21, 22, 23, 24, 25, 26, 27]. One technique in order to increase the heat transfer rate is the optimization of the heat exchanger geometry [20, 21, 22]. Another way in order to increase the heat transfer rate is to increase the heat transfer coefficient, reducing the hydraulic diameter of the channel, or to use corrugated (or rough) channel walls. These methods are used in order to increase the thermal performance of the heat transfer device. When the dimensions of the exchanger channels reach a size in the micro- or nano-meter range, laminar flow conditions should apply as the pressure drop becomes excessively high [17, 18]. At this stage, during design process, additional filters removing impurities from the working fluid have to be considered [1, 2, 3, 4, 23, 24, 25, 26, 27]. In addition, during the modelling stage of the heat exchanger with micro- and nano-channels, slip on the channel walls phenomena should be included. At the nano-scale, this slip effect on the

*Corresponding author
Email address: skornet@imp.gda.pl (Sebastian Kornet)

wall is a very important issue which has been described in many papers [28, 29, 30, 31, 32, 33, 34].
In many applications, heating and cooling of solid structures and maintaining thermal boundary conditions are directly coupled to the solid and fluid interface. Therefore, during the design process the thermal interaction between the working fluid and the solid structure should be taken into account [35, 36, 37]. Thermal-FSI ("Fluid Solid Interaction") tools can be efficiently used for such a full coupled thermal fluid flow and thermal structure analysis [38, 39].
Nowadays, the numerical analysis allows to: determine the temperature in situations where local temperature measurements are difficult to obtain [40, 41, 42, 43], select the correct grade of material for each of the sub-components [44, 45, 46, 47], a suitable selection of the wall thickness and corresponding shapes at the design stage [20, 21, 22], assess the viability of components, and an on-line monitoring of the thermal stresses [48, 49, 50].
In this paper selected numerical modelling problems for an advanced thermal-FSI ("Fluid Solid Interaction") mini-channel heat exchanger model are presented. Special attention is given to the heat transfer between the separated mediums for different mass flows. Basic tests, including a comparison with experimental data, have been conducted using a Mini-channel Plate Heat Exchanger (MPHE). The thermal-FSI analysis was applied for the heat exchanger model with one hot and one cold water flow passage through the mini-channels. Satisfactory aggreement between the modelling results and the experimental data [4] was obtained.

2. Geometry and discretization of heat exchanger with mini-channels

In order to conduct a thermal-FSI analysis, I version of the MPHE geometry was selected:a heat exchanger with unmodified mini-channels. A 3D geometrical model of a mini-channel heat exchanger made out of two gasketed brazed plates with 40 mm long rectangular cross section channels (width—1 mm, depth—700 μm) was built with one closing plate and two fluid domains. The distance between the mini-channels was 1 mm, and the heat transfer area was 0.00694 m^2. The full geometry of the analyzed heat exchanger with mini- channels (which includes the fluid and the solid domains) adopted to thermal-FSI simulations is shown in Fig. 1. Inlets, outlets, and flow directions of the working fluids are highlighted in Fig. 1. Details of the MPHE geometry and the experiment carried out by Mikielewicz and Wajs in 2017 can be found in reference [4]. In order to better discretize the process, the geometry of the collector zone which contributed to the creation of the higher quality mesh was simplified. The 3D MPHE model (which contains solid and fluid domains) was discretized using a finite volume method (FVM). The FVM discretization of a solid plate with mini-channels is presented in Fig. 2a. In the fluid domains, the grid size of the mini-channel zones were decreased. Please see magnified details in Fig. 2b. All results considered in this work are presented in two planes which cross the plates of

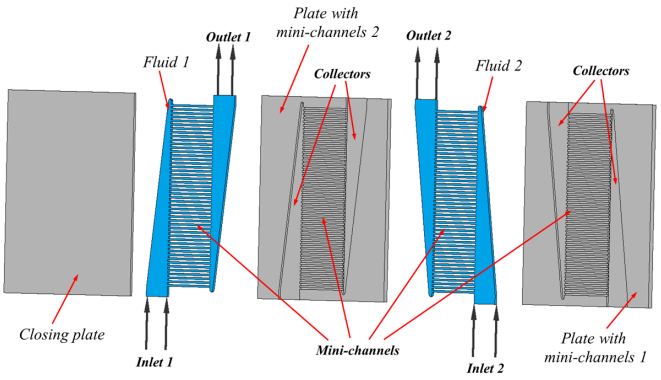

Figure 1: Full 3D geometry of the MPHE (including fluids and solids domains) adopted to Thermal-FSI analysis with highlighted inlets, outlets and flow directions for the working fluid

the MPHE at the middle section of the mini-channels height. The first plane (in this work called cold plane) crosses the mini-channel plate with the cold (or heating) fluid domain. The second plane (in this article called hot plane) crosses the mini-channel plate which includes the heating (or cooling) fluid domain.

3. Thermal-FSI approach

The thermal-FSI analysis is a part of the science dedicated to describe of energy transport and conversion within a thin layer occurring in a contact with the solid and the fluid [2, 51]. With the thermal-FSI approach, the basic assumption is that both, the solid deformation and the fluid flow, are governed by the same kind of momentum conservation which should be adequately expressed for an effective fluid-solid thermal energy exchange [52, 53, 54]. This assumption means that the momentum and the energy equations are solved using the same grid for both, the solid and the fluid. In difference to the Momentum-FSI (more information on the momentum-FSI can be found in [55, 56, 57]), where the exchange of momentum between solid and fluid is the main phenomena, the thermal-FSI equation for the energy plays the main role in both directions (from solid to fluid and vice versa) of energy transport [2]. In thermal-FSI flow equations (for the fluid domain) are solved by a CFD (Computational Fluid Dynamics) solver, the response of the solid body is obtained by using a CSD (Computational Solid Dynamics) solver.

3.1. The set of CFD balance equations

In fluid domain the starting point for the CFD computation is to define a universal set of mass, momentum and energy balance equations for the fluid as followed:

- balance of mass—ρ:

$$\partial_t(\rho) + \mathrm{div}(\rho \mathbf{v}) = 0 \tag{1}$$

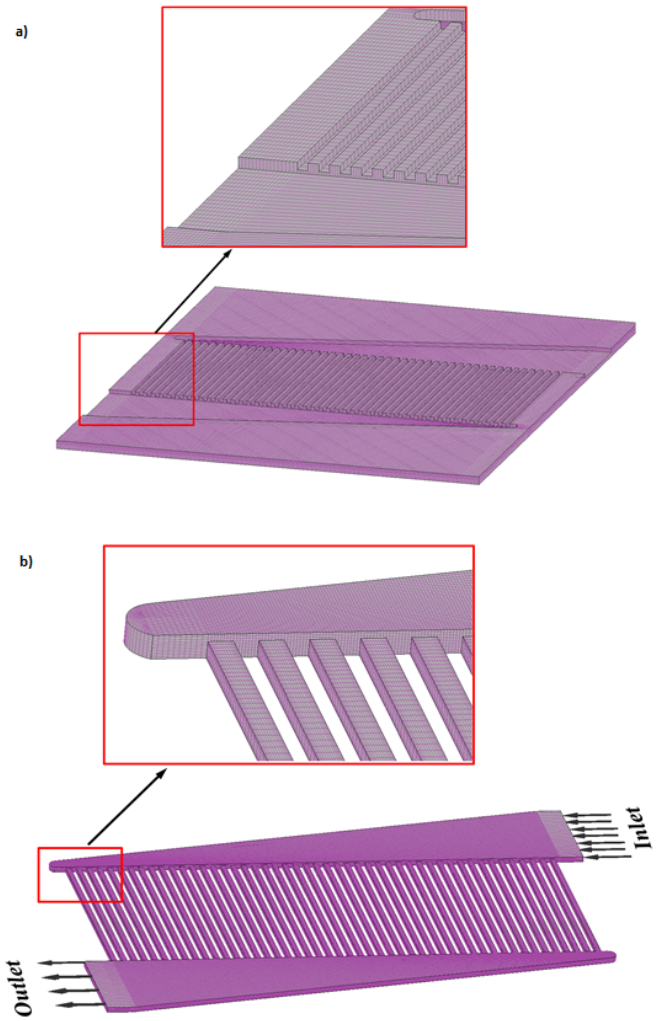

Figure 2: FVM discretization of: a) the solid plate with mini-channels, b) the working fluid domain with highlighted flow direction

- balance of momentum—$\rho\mathbf{v}$:

$$\partial_t(\rho\mathbf{v}) + \mathrm{div}(\rho\mathbf{v}\otimes\mathbf{v} + p\mathbf{I}) = \mathrm{div}(\tau^c) + \rho\mathbf{b} \tag{2}$$

- balance of energy—e:

$$\partial_t(\rho e) + \mathrm{div}(\rho e\mathbf{v} + p\mathbf{v}) = \mathrm{div}\left(\tau^c\mathbf{v} + \mathbf{q}^C_{fluid}\right) + \rho\mathbf{b}\cdot\mathbf{v} \tag{3}$$

where: $\rho = \rho(\mathbf{x}, t)$—fluid density, which generally dependents on the time t and the location $\mathbf{x}$, $\mathbf{v} = v_i\mathbf{e}_i$—fluid velocity, p—thermodynamical pressure, $\mathbf{I} = \delta_{ij}\mathbf{e}_i \otimes \mathbf{e}_j$—unity tensor, $\tau^c = \tau + \mathbf{R} + \mathbf{D}$—the viscous, turbulent and diffusive flux of momentum, $\mathbf{b}$—mass force of Earth gravity, $e = u + \frac{v^2}{2}$—which is the sum of the internal and kinetic energy, $\mathbf{q}^C_{fluid} = \mathbf{q} + \mathbf{q}^+ + \mathbf{q}^{ph} + ...$—total heat flux in the fluid. In order to take into account the influence of turbulent transport of the momentum and the turbulent transport of heat, the fluid should possess a set of additional equations governing the evolution for turbulent primary parameters, for instance turbulent kinetic energy k and turbulent dissipation energy ω [56, 57]:

$$\partial_t(\rho k) + \mathrm{div}(\rho k\mathbf{v}) = \mathrm{div}(\mathbf{J}_k) + S_k \tag{4}$$

$$\partial_t(\rho\omega) + \mathrm{div}(\rho\omega\mathbf{v}) = \mathrm{div}(\mathbf{J}_\omega) + S_\omega \tag{5}$$

where: $\mathbf{J}_k$, $\mathbf{J}_\omega$—diffusive flux of k and diffusive flux of ω with sources S_k, S_ω (various definitions from different authors exist in the literature). For each finite volume of the computational grid seven equations were solved (one for mass, energy, k and ω transport balance equation and three momentum balance equations). The five balance equation (which consist of one mass balance equation, three momentum balance equations and one energy balance equation) and two evolution equations for parameters defining turbulence (equation for turbulent kinetic energy evolution k and equation for turbulence dissipation evolution ω) have been described by Badur [3, 51, 58]. The turbulent viscosity in (4) and (5) is computed by combining k and ω as follows [1, 3, 51, 57, 58]:

$$\mu_t = \alpha^*\frac{\rho k}{\omega} \tag{6}$$

For low fluid velocities (laminar-turbulent transitions) the coefficient α^* damps the turbulent viscosity causing a low Re_t number correction. It is given by [1, 3, 51, 57, 58]:

$$\alpha^* = \alpha^*_\infty\left(\frac{\alpha^*_0 + Re_t/R_k}{1 + Re_t/R_k}\right) \tag{7}$$

where: $\alpha^*_0 = 0.024$, $R_k = 6$, $Re_t = \frac{\rho k}{\mu\omega}$. For full turbulent flows the coefficient α^* is equal 1.

3.2. The set of CSD balance equations

In analogy to the CFD set of governing equations, the appropriate set of CSD governing equations is determined as followed [2, 55, 56]:

- balance of mass—ρ:

$$\partial_t(\rho) + \mathrm{div}(\rho\mathbf{v}) = 0 \tag{8}$$

- balance of momentum—$\rho\mathbf{v}$:

$$\partial_t(\rho\mathbf{v}) + \mathrm{div}(\rho\mathbf{v}\otimes\mathbf{v}) = \mathrm{div}(\sigma) + \rho\mathbf{b} \tag{9}$$

- balance of energy—e:

$$\partial_t(\rho e) + \mathrm{div}(\rho e\mathbf{v}) = \mathrm{div}\left(\sigma\mathbf{v} + \mathbf{q}^C_{solid}\right) + S_e \tag{10}$$

where: σ—elastic stress tensor, $\mathbf{q}^C_{solid}$—total heat flux in the solid, S_e—source. To the set of CSD governing equations, an additional evolution equations describing the behavior of the solid material can be added e.g.: evolution of plastic strain, evolution of kinematic hardening, evolution of isotropic hardening etc. [55, 56]. Here, CSD is a point-blank analogy for CFD (Computational Fluid Dynamics). Both methods use the same balance equations (mass, momentum and energy). A discretization method for the CSD and CFD is arbitrary (FEM, FVM, etc.) but the governing equations are identical. This architecture, solving the equation, greatly simplifies the thermal-FSI analysis [56].

The CSD analysis mostly allows to determine the materials deformation, stresses and the structural changes in materials due to the heating or cooling process. The material strain along the contact line with the fluid wall should be fully coupled. For this reasons, a re-meshing or a moving mesh method should be used.

In our case, the maximum temperature of the fluid is relatively low (below 100°C), for which reason it is assumed that the deformations of the MPHE plates are small too, allowing to skip the momentum and the mass balance consideration for the solid body. This assumption causes the thermal-FSI analysis to couple only in one way (from the fluid to the solid domain).

3.3. Coupling energy balance equation in the fluid-solid contact layer

When analysing the transport of heat across the solid-fluid contact layer, one should consider the exact nature of a nonlinear equation for the thermal motion. In practice, the balance of energy (equation (3) for the fluid domain and equation (10) for the solid domain) is the governing equation for the field of temperature $T = T(\mathbf{x}, t)$. According to the principle of producing energy "ex nihilo" in the energy equation, there is no internal sources of energy and the change of energy e is the only governing energy flux. The most important flux describing the thermal motion is the dynamics of the Stokes-Rankine heating energy flux heat: $\mathbf{q}_f^C$—for fluids and $\mathbf{q}_f^C$—for solid materials [2, 58].

State of the art thermal-FSI has no possibilities for numerical solution of the full energy balance within the thermal contact layer (equation 8 in [2]). The first reason is the insufficient development of the Finite Element Method as well as of the Finite Volume Method [2, 58]. Actually, both methods are prepared only in order to solve simultaneously only one part of the equation in the following form:

$$\mathbf{q}_f^C \cdot \mathbf{n}_f + \mathbf{q}_s^C \cdot \mathbf{n}_s = \mathbf{0} \tag{11}$$

where: $\mathbf{n}_f$ and $\mathbf{n_s}$ are normal vectors for the fluid and the solid, respectively. Applying the thermal-FSI by coupling the energy balance within the thermal contact layer in this simplified approach is shown in Fig. 3. The total heat flux through the contact layer between the fluid and the solid can be determined as followed [59]:

$$\mathbf{q}_f^C = \lambda^f \mathrm{grad}(T) \tag{12}$$

$$\mathbf{q}_s^C = \lambda^s \mathrm{grad}(T) \tag{13}$$

The thermal-FSI is based on the concept of functionally changing the heat diffusion coefficients (thermal conductivity) to the nearest neighbouring of the surface contact, for instance $\lambda^f = \lambda^f(Re, y^+, \delta, etc.)$ [2, 58]. More details about heat flux components can be found in [1, 2, 3, 51, 58].

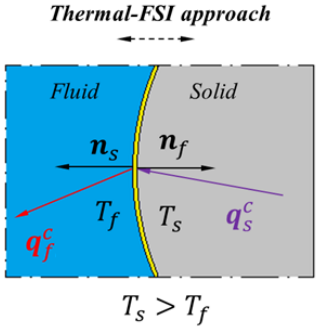

Figure 3: Realization of Thermal-FSI by coupling of energy balance within the thermal contact layer, where: $\mathbf{q}_s^C$—total diffusive heat flux in the solid body; $\mathbf{q}_f^C$—total diffusive heat flux in the fluid domain; T_s—solid temperature; T_f—fluid temperature; $\mathbf{n}$—normal vector

Table 1: Boundary conditions adopted to Thermal-FSI analysis of the MPHE, where: $T_c^{'}$—cold fluid temperature at the inlet; $T_h^{'}$—hot fluid temperature at the inlet; $\dot{V}_c$—volume flow rate of cold fluid; $\dot{V}_h$—volume flow rate of hot fluid

	Cold side		Hot side	
Case	$T_c^{'}$, °C	$\dot{V}_c$, l/h	$T_h^{'}$, °C	$\dot{V}_h$, l/h
I	9.1	50	92.6	50
II	7.4	250	91.8	250
III	6.6	500	92.9	400

4. Boundary conditions adopted to Thermal-FSI analysis

Modelling conditions have been taken from the description of an experiment [4], originally conducted at the Gdansk University of Technologies. In the presented paper, special attention is given to the heat transfer between the separated mediums for different mass flows. The thermal-FSI analysis has been conducted in the model for the heat exchanger consisting of one hot and one cold passage of the water passing through mini-channels between the plates. The basic tests includes a comparison with experimental data which have been obtained using the I version of the MPHE geometry. The boundary conditions adopted by the thermal-FSI analysis are shown in Table 1. For case I of boundary conditions, a numerical analysis with a laminar flow was performed. For the remaining cases, the performed simulation uses a k-ω SST turbulence model with a low Reynolds number correction. More details about the experiment and the experimental conditions can be found in [4].

5. Results of Thermal-FSI analysis and comparison with experimental data

For the geometry of the MPHE shown in the Fig. 1, the thermal-FSI analysis has been conducted in the model for one hot and one cold water passage through the mini-channels which housed in plates. The thermal-FSI analysis includes the heat transfer between the separated mediums

for different mass flows. The analysis was conducted for a counter-current flow of the working fluids (hot and cold water), identical to the experiment. The numerical results are as followed: the hot fluid temperature at the outlet of the heat exchanger, the cold fluid temperature at the outlet of the heat exchangers and heat flux, were compared with the experimental data. The results are expressed in local and integral form. For the integral interpretation, the equation for the heat flux is defined as [60]:

$$\dot{Q} = c_p \dot{V} \rho (T_h^{'} - T_h^{''}) \tag{14}$$

where: c_p—specific heat capacity at constant pressure [kJ/kgK]; $\dot{V}$—volume flow rate [m^3/s]; ρ—density [kg/m^3]; $T_h^{'}$—hot fluid temperature at the inlet [K]; $T_h^{''}$—hot fluid temperature at the outlet [K]. Similar definition of the equation (14) was used in [61, 62, 63] in order to determine the energy balance of the heat exchanger using numerical or analytical calculations. However, the formulation mentioned above is also corrected determining the total rate of the heat transfer between the two fluids for the experimental results [17, 23, 35] (this works also describes a similar experiment).

In Fig. 4a and 4b show the temperature distribution for case I with the corresponding boundary conditions for the cold plane and the hot plane. Inlets for both, hot and cold water, are located at the bottom of the figures. Results for the remaining cases are presented in the same way as in Fig. 4. Temperature distributions on the cold plane and the hot plane for the cases II and III with the corresponding boundary conditions are shown in Fig. 5 and Fig. 6, respectively.

Independently from the boundary conditions, the hot fluid is cooling and the cold fluid is being heated. This is particularly noticeable in the mini-channels zones (see Fig. 4a and 4b below). The cold fluid temperature is the biggest in the regions close to the mini-channel walls at the outlet to the outlet collector (see Fig. 4a below). In the central zone of the cold mini-channel, the water temperature is still low (Fig. 4a below). Hence, the outlet collector zone we can be considered as a “cold jet” heating the fluid (see Fig. 4a above). The same phenomena is noticeable for the hot water. Thermal-FSI results shows that for the analyzed MPHE the hydraulic diameter of the channels can be reduced in order to enhancement the heat transfer, but this approach can leads to a significant increase in pumping power. The numerical results also show that with an increasing mass flow the outlet temperature of the hot water is higher and the outlet temperature of the cold water lower.

Table 2 presents the numerical and experimental results for the outlet temperatures (both for hot and cold water) for all cases considered . Additionally, the table presents the results of the heat flux transferred in the MPHE for all cases of boundary conditions. Results (both outlet temperatures and heat fluxes) obtained using thermal-FSI tool agree very well with the experimental data for all cases analyzed .

The maximum difference for the outlet temperature between the thermal-FSI results and the experimental data exists for case I, but this difference does not exceed 2.35°C for the cold water. Maximum deviation of the heat flux is equal to 0.22 kW for the case II boundary conditions. In this experiment, the measurement error for the outlet and inlet temperatures was equal to 0.5°C; for the mass fluxes was equal to approximately 3.5% of the measured mass flow rate. More details about the measurement errors can be found in [4].To minimize simulation errors, the mini-channels and collectors were divided into blocks and discretized by means of a structured numerical grid, steeply refined towards the normal wall direction. Initial tests confirmed the use of the numerical grid ensuring that further refinement does not influence the computational results. It was assumed that the MPHE is ideally isolated. Additionally the surface structure of the mini-channels was treated as homogeneous. It should also be added that the standard SIMPLE (semi-implicit method for pressure-linked equations) method was used for the pressure-velocity coupling. The second order upwind schemes have been employed for the solution of the convection term in the governing equations. The diffusion terms have been centrally differenced with a second order accuracy. The detailed methodology of the numerical integration regarding the set of governing equations can be found in the following work [3, 58]. In order to better determine the heat flux in the mini-channels zone, the fluid domain was divided into three subdomains: the inlet collector, the mini-channels zone and the outlet collector (see Fig. 7). In each subdomain the heat flux was determined using the equation 14. The numerical results of the heat flux in all subdomains for all considered cases of boundary conditions are presented in Table 3. The biggest heat flux occurs in the mini-channels zone for all considered cases. The heat flux in the mini-channels zone with respect to the total heat flux is approximately equal: 75% for case I, 70% for case II and 67% for case III. When increasing the mass flow, the heat flux in the mini-channels zone also increase. However, results obtained with the thermal-FSI show that when increasing the mass flow the contribution of the heat flux in the mini-channels zone decreases with respect to total heat flux.

Thermal-FSI analysis shows, as expected, that the regions of the enhanced heat transfer are located in the mini-channels of the analyzed heat exchanger. The localization of the enhancement heat transfer zone between the working fluids in the MPHE is obtained by using the thermal-FSI analysis as shown in Fig. 8. Our numerical thermal-FSI analysis confirms the assumption that a decrease in hydraulic dimension of channels leads to an increase in heat transfer with the MPHE.

6. Conclusion

In this work the authors conducted a numerical analysis of a MPHE geometry model for different boundary conditions. The results obtain with the thermal-FSI tool agree very well with the experimental data for all cases considered. Good agreement with the experiment has been obtained for both, outlet temperatures and heat fluxes. Maximum deviation of

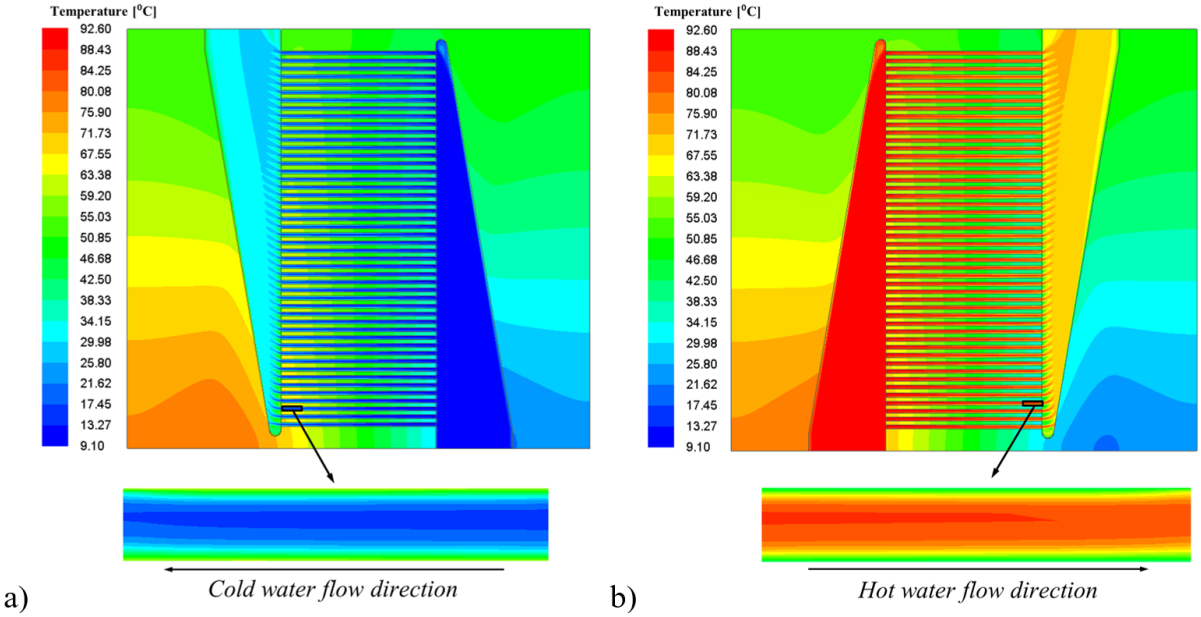

Figure 4: The temperature distribution on: a) the cold plane and b) the hot plane for the case I of boundary conditions (laminar flow)

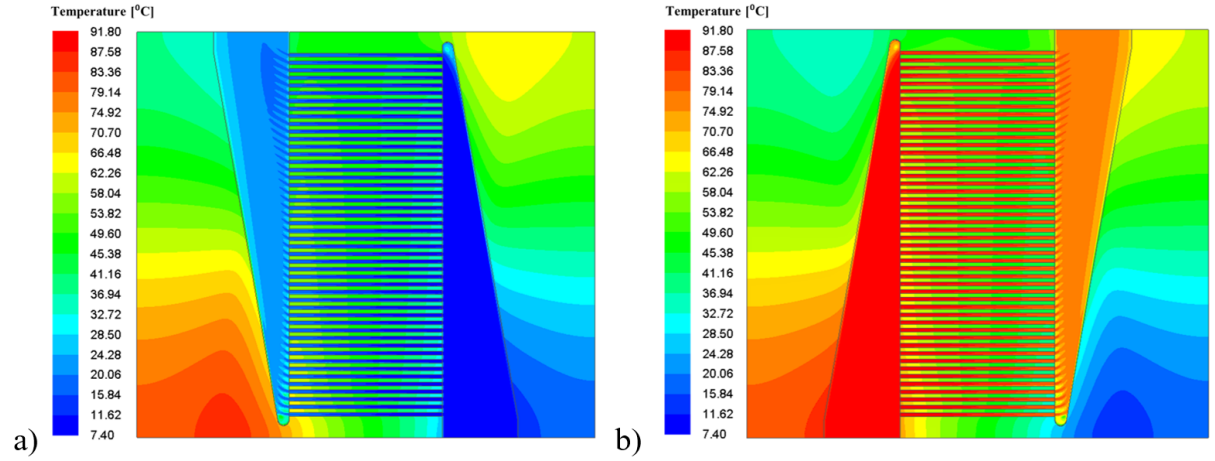

Figure 5: The temperature distribution on: a) the cold plane and b) the hot plane for the case II of boundary conditions (turbulent flow with low-Re number correction)

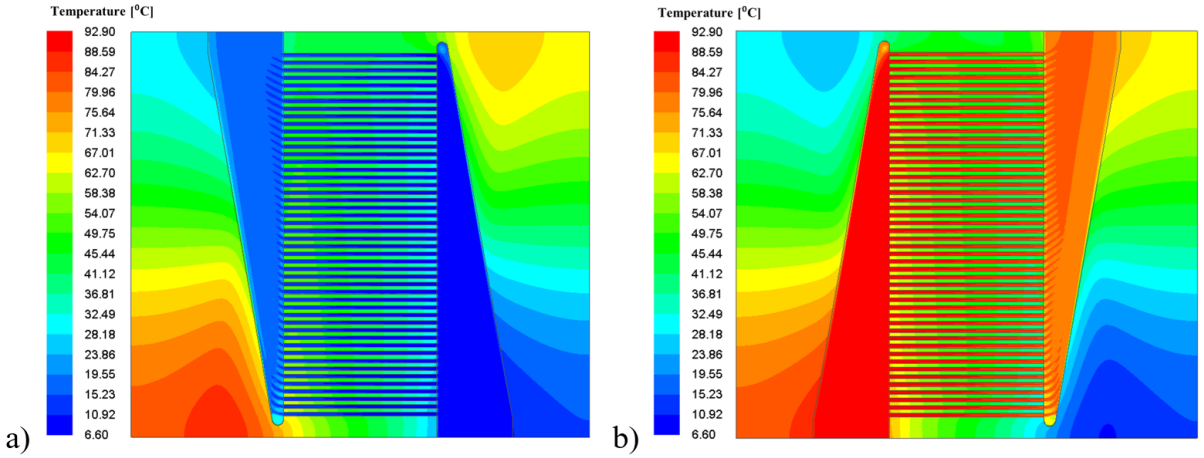

Figure 6: The temperature distribution on: a) the cold plane and b) the hot plane for the case III of boundary conditions (turbulent flow with low-Re number correction)

Table 2: Comparison between numerical results obtained with the Thermal-FSI analysis and with the experimental data, where: $T_c^{'}$—cold fluid temperature at the inlet; $T_c^{''}$—cold fluid temperature at the outlet; $T_h^{'}$—hot fluid temperature at the inlet; $T_h^{''}$—hot fluid temperature at the outlet; $\dot{V}_c$—volume flow rate of cold fluid; $\dot{V}_h$—volume flow rate of hot fluid; $\dot{Q}$—heat flux

		Cold side			Hot side			
Case		$\dot{V}_c$, l/h	Inlet $T_c^{'}$, °C	Outlet $T_c^{''}$, °C	$\dot{V}_h$, l/h	Inlet $T_h^{'}$, °C	Outlet $T_h^{''}$, °C	$\dot{Q}$, kW
Experiment	I	50±1.8	9.1±0.5	37.6±0.5	50±1.8	92.6±0.5	64.7±0.5	1.64
Thermal-FSI	I	50	9.1	35.28	50	92.6	65.38	1.53
Experiment	II	250±9	7.4±0.5	22±0.5	250±9	91.8±0.5	76.9±0.5	4.24
Thermal-FSI	II	250	7.4	22.71	250	91.8	75.81	4.45
Experiment	III	500±18	6.6±0.5	17.5±0.5	400±14.4	92.9±0.5	79.5±0.5	6.21
Thermal-FSI	III	500	6.6	17.37	400	92.9	78.67	6.27

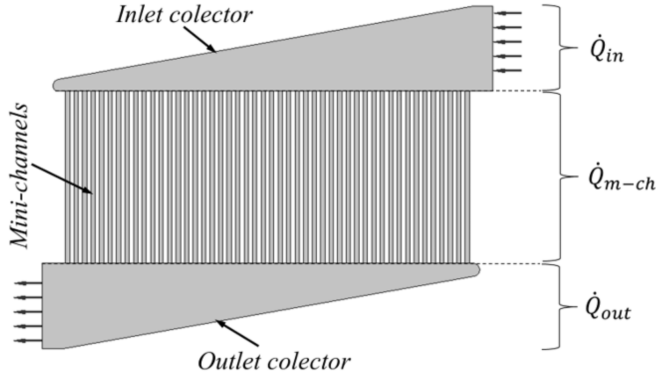

Figure 7: Fluid domain divided into three subdomains: the inlet collector, the mini-channels zone and the outlet zone, where: $\dot{Q}_{in}$—the heat flux in the inlet collector; $\dot{Q}_{m-ch}$—the heat flux in the mini-channels zone; $\dot{Q}_{out}$—the heat flux in the outlet collector; $\dot{Q}$—total heat flux

Table 3: Thermal-FSI results of the heat flux in selected subdomains, where: $\dot{Q}_{in}$—the heat flux in the inlet collector; $\dot{Q}_{m-ch}$—the heat flux in the mini-channels zone; $\dot{Q}_{out}$—the heat flux in the outlet collector; $\dot{Q}$—total heat flux

Case	$\dot{Q}_{in}$, kW	$\dot{Q}_{m-ch}$, kW	$\dot{Q}_{out}$, kW	$\dot{Q}$, kW
I	0.33	1.15	0.05	1.53
II	1.13	3.08	0.24	4.45
III	1.61	4.23	0.43	6.27

the outlet temperature does not exceed 2.35°C. As expected, the thermal-FSI analysis showed that the heat transfer in the MPHE exchanger geometry is the biggest in the mini-channels zone for all cases considered.

Good agreement with the experiment indicate that the thermal-FSI tool can be efficiently used for a fully coupled thermal fluid flow and with a thermal structural analysis. But for cases when changes in temperature lead to significant thermal deformation in solid bodies, additional re-meshing or a moving mesh method should be used.

Acknowledgements

The work results were obtained in studies co-financed by National Research and Development Center in the project PBS 3 ID 246201 titled: The development of innovative technology, thin foils of alloys based on intermetallic phase Ni3Al with high activity thermocatalytic in the field of purification of air from harmful substances or controlled decomposition of hydrocarbons.

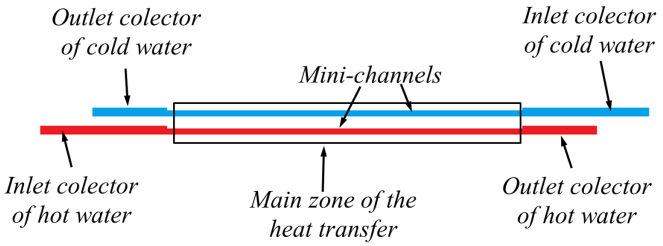

Figure 8: Localization of enhancement heat transfer zone between working fluids in the MPHE exchanger obtained by using thermal-FSI analysis

References

[1] J. Badur, H. Charun, Selected problems of heat exchange modelling in pipe channels with ball turbulisers, Archives of Thermodynamics 28 (1) (2007) 65–88.

[2] J. Badur, P. Ziółkowski, W. Zakrzewski, D. Sławiński, S. Kornet, T. Kowalczyk, J. Hernet, R. Piotrowski, J. Felincjancik, P. Ziółkowski, An advanced thermal-fsi approach to flow heating/cooling, in: Journal of Physics: Conference Series, Vol. 530, IOP Publishing, 2014, p. 012039.

[3] J. Badur, Five lectures of contemporary fluid thermomechanical fluids, 2 edition, Gdańsk, (in Polish) (2005).

[4] D. Mikielewicz, J. Wajs, Possibilities of heat transfer augmentation in heat exchangers with minichannels for marine applications, Polish Maritime Research 24 (s1) (2017) 133–140.

[5] A. M. Adham, N. Mohd-Ghazali, R. Ahmad, Thermal and hydrodynamic analysis of microchannel heat sinks: A review, Renewable and Sustainable Energy Reviews 21 (2013) 614–622.

[6] A. Bejan, A. D. Kraus, Heat transfer handbook, Vol. 1, John Wiley & Sons, 2003.

[7] T. Dixit, I. Ghosh, Review of micro-and mini-channel heat sinks and heat exchangers for single phase fluids, Renewable and Sustainable Energy Reviews 41 (2015) 1298–1311.

[8] M. Feidt, Finite Physical Dimensions Optimal Thermodynamics 1 Fundamentals, ISTE Press /Elsevier, 2017.

[9] Y. Han, Y. Liu, M. Li, J. Huang, A review of development of microchannel heat exchanger applied in air-conditioning system, Energy Procedia 14 (2012) 148–153.

[10] Q. Li, G. Flamant, X. Yuan, P. Neveu, L. Luo, Compact heat exchangers: A review and future applications for a new generation of high temperature solar receivers, Renewable and Sustainable Energy Reviews 15 (9) (2011) 4855–4875.

[11] F. Pra, P. Tochon, C. Mauget, J. Fokkens, S. Willemsen, Promising designs of compact heat exchangers for modular htrs using the brayton cycle, Nuclear Engineering and Design 238 (11) (2008) 3160–3173.

[12] J. Hesselgreaves, Compact Heat Exchangers: Selection, Design and Operation, Gulf Professional Publishing, 2001.
[13] J. Madejski, Theory of heat transfer, Szczecin University of Technology, Szczecin.
[14] E. P. Gyftopoulos, G. P. Beretta, Thermodynamics: foundations and applications, Courier Corporation, 2005.
[15] A. C. Caputo, P. M. Pelagagge, P. Salini, Heat exchanger optimized design compared with installed industrial solutions, Applied Thermal Engineering 87 (2015) 371–380.
[16] M. M. A. Bhutta, N. Hayat, M. H. Bashir, A. R. Khan, K. N. Ahmad, S. Khan, Cfd applications in various heat exchangers design: A review, Applied Thermal Engineering 32 (2012) 1–12.
[17] L. S. Ismail, R. Velraj, C. Ranganayakulu, Studies on pumping power in terms of pressure drop and heat transfer characteristics of compact plate-fin heat exchangers—a review, Renewable and Sustainable Energy Reviews 14 (1) (2010) 478–485.
[18] W. Dahmen, S. Müller, M. Rom, S. Schweikert, M. Selzer, J. von Wolfersdorf, Numerical boundary layer investigations of transpiration-cooled turbulent channel flow, International Journal of Heat and Mass Transfer 86 (2015) 90–100.
[19] M. Khoshvaght-Aliabadi, F. Nozan, Water cooled corrugated minichannel heat sink for electronic devices: Effect of corrugation shape, International Communications in Heat and Mass Transfer 76 (2016) 188–196.
[20] C. Fernandes, R. Dias, J. Nobrega, J. Maia, Laminar flow in chevron-type plate heat exchangers: Cfd analysis of tortuosity, shape factor and friction factor, Chemical Engineering and Processing: Process Intensification 46 (9) (2007) 825–833.
[21] M. Saeed, M.-H. Kim, Header design approaches for mini-channel heatsinks using analytical and numerical methods, Applied Thermal Engineering 110 (2017) 1500–1510.
[22] K. Śmierciew, M. Kołodziejczyk, J. Gagan, D. Butrymowicz, Numerical modelling of fin heat exchanger in application to cold storage, Heat Transfer Engineering (just-accepted).
[23] G. A. Jaglarz, D. Taler, Experimental study of fouling in plate heat exchangers in district heating systems, Journal of Power Technologies 95 (5) (2015) 42.
[24] R. Mastrullo, A. Mauro, R. Revellin, L. Viscito, Modeling and optimization of a shell and louvered fin mini-tubes heat exchanger in an orc powered by an internal combustion engine, Energy Conversion and Management 101 (2015) 697–712.
[25] B. Agostini, B. Watel, A. Bontemps, B. Thonon, Friction factor and heat transfer coefficient of r134a liquid flow in mini-channels, Applied Thermal Engineering 22 (16) (2002) 1821–1834.
[26] T. Morosuk, C. Morosuk, M. Feidt, New proposal in the thermodynamic analysis of complex heat regeneration systems, Energy 29 (12) (2004) 2517–2535.
[27] V. Dvořák, T. Vít, Evaluation of cae methods used for plate heat exchanger design, Energy Procedia 111 (2017) 141–150.
[28] J. Badur, M. Karcz, M. Lemański, On the mass and momentum transport in the navier–stokes slip layer, Microfluidics and Nanofluidics 11 (4) (2011) 439–449.
[29] J. Badur, P. Ziółkowski, W. Zakrzewski, D. Sławinski, M. Banaszkiewicz, O. Karczmarczyk, S. Kornet, P. Ziółkowski, On the surface vis impressa caused by a fluid-solid contact, Shell Structures: Theory and Applications 3 (2013) 53.
[30] J. Badur, P. J. Ziółkowski, P. Ziółkowski, On the angular velocity slip in nano-flows, Microfluidics and Nanofluidics 19 (1) (2015) 191–198.
[31] S. Cano-Andrade, G. P. Beretta, M. R. von Spakovsky, Non-equilibrium thermodynamic modeling of an atom-field state evolution with comparisons to published experimental data, in: Proceedings of the 12th Joint European Thermodynamics Conference, Brescia, Italy, 2013, pp. 1–5.
[32] S. Sanaye, M. Dehghandokht, Thermal modeling of mini-channel and laminated types evaporator in mobile air conditioning system, International Journal of Automotive Engineering 2 (2) (2012) 68–83.
[33] B. Salman, H. Mohammed, K. Munisamy, A. S. Kherbeet, Characteristics of heat transfer and fluid flow in microtube and microchannel using conventional fluids and nanofluids: a review, Renewable and Sustainable Energy Reviews 28 (2013) 848–880.
[34] P. Ziółkowski, J. Badur, Navier number and transition to turbulence, in: Journal of Physics: Conference Series, Vol. 530, IOP Publishing, 2014, p. 012035.
[35] S. Alfarawi, R. Al-Dadah, S. Mahmoud, Transient investigation of mini-channel regenerative heat exchangers: Combined experimental and cfd approach, Applied Thermal Engineering 125 (2017) 346–358.
[36] P. Ziółkowski, J. Badur, On the unsteady reynolds thermal transpiration law, in: Journal of Physics: Conference Series, Vol. 760, IOP Publishing, 2016, p. 012041.
[37] M. T. Mabrouk, A. Kheiri, M. Feidt, Using generalized integral transforms to solve a perturbation model for a packed bed thermal energy storage tank, International Journal of Heat and Mass Transfer 84 (2015) 633–641.
[38] J. Badur, P. Ziółkowski, D. Sławiński, S. Kornet, An approach for estimation of water wall degradation within pulverized-coal boilers, Energy 92 (2015) 142–152.
[39] J. Badur, P. Ziolkowski, S. Kornet, M. Stajnke, M. Bryk, K. Banas, P. Ziolkowski, The effort of the steam turbine caused by a flood wave load, in: AIP Conference Proceedings, Vol. 1822, AIP Publishing, 2017, p. 020001.
[40] A. E. Quintero, M. Vera, Laminar counterflow parallel-plate heat exchangers: An exact solution including axial and transverse wall conduction effects, International Journal of Heat and Mass Transfer 104 (2017) 1229–1245.
[41] D. Taler, P. Ocłoń, Thermal contact resistance in plate fin-and-tube heat exchangers, determined by experimental data and cfd simulations, International Journal of Thermal Sciences 84 (2014) 309–322.
[42] X. Liu, J. Yu, Numerical study on performances of mini-channel heat sinks with non-uniform inlets, Applied Thermal Engineering 93 (2016) 856–864.
[43] O. Giurgiu, A. Pleşa, L. Socaciu, Plate heat exchangers–flow analysis through mini channels, Energy Procedia 85 (2016) 244–251.
[44] P. Madejski, D. Taler, Analysis of temperature and stress distribution of superheater tubes after attemperation or sootblower activation, Energy conversion and management 71 (2013) 131–137.
[45] J. Fu, L. Wei, N. Li, Q. Zhou, T. Liu, Experimental study on temperature, heat flux, strain and stress distribution of boiler water walls, Applied Thermal Engineering 113 (2017) 419–425.
[46] Y. Rouizi, W. Al Hadad, D. Maillet, Y. Jannot, Experimental assessment of the fluid bulk temperature profile in a mini channel through inversion of external surface temperature measurements, International Journal of Heat and Mass Transfer 83 (2015) 522–535.
[47] M. Costea, M. Feidt, The effect of the overall heat transfer coefficient variation on the optimal distribution of the heat transfer surface conductance or area in a stirling engine, Energy conversion and management 39 (16) (1998) 1753–1761.
[48] J. Taler, P. Duda, B. Węglowski, W. Zima, S. Grądziel, T. Sobota, D. Taler, Identification of local heat flux to membrane water-walls in steam boilers, Fuel 88 (2) (2009) 305–311.
[49] M. Banaszkiewicz, On-line monitoring and control of thermal stresses in steam turbine rotors, Applied Thermal Engineering 94 (2016) 763–776.
[50] J. Taler, B. Węglowski, P. Dzierwa, P. Czupryński, P. Madejski, D. Nabagło, C. Żyrkowski, Analysis to speed up of the start-up of steam boiler op-380, Journal of Power Technologies 94 (2) (2014) 1–8.
[51] J. Felicjancik, P. Ziółkowski, J. Badur, An advanced thermal-fsi approach of an evaporation of air heat pump, Transactions of the Institute of Fluid-Flow Machinery (129) (2015) 111–141.
[52] B. D. Coleman, W. Noll, The thermodynamics of elastic materials with heat conduction and viscosity, Archive for Rational Mechanics and Analysis 13 (1) (1963) 167–178.
[53] C. Truesdell, Rational Thermodynamics, 2nd ed., Springer-Verlag, 1984.
[54] V. Eremeyev, W. Pietraszkiewicz, Thermomechanics of shells undergoing phase transition, Journal of the Mechanics and Physics of Solids 59 (7) (2011) 1395–1412.
[55] J. Badur, S. Kornet, D. Sławiński, P. Ziółkowski, M. Banaszkiewicz, A. Rehmus-Forc, Numerical analysis of cracking hazard of a thermowell for measuring steam temperature in a steam turbine control stage, Journal of Power Technologies 96 (6) (2016) 361–367.
[56] S. Kornet, D. Sławiński, P. Ziółkowski, J. Badur, Analysis of unsteady flow forces on the thermowell of steam temperature sensor, Transactions of the Institute of Fluid-Flow Machinery.

[57] D. C. Wilcox, et al., Turbulence modeling for CFD, Vol. 2, DCW industries La Canada, CA, 1998.
[58] J. Badur, Numerical modeling of sustainable combustion in gas turbines, IFFM PAS, Gdańsk.
[59] J. B. J. Baron Fourier, The analytical theory of heat, The University Press, 1878.
[60] A. Bejan, Entropy generation minimization, CRC, 1996.
[61] M. Blaise, M. Feidt, D. Maillet, Optimization of the changing phase fluid in a carnot type engine for the recovery of a given waste heat source, Entropy 17 (8) (2015) 5503–5521.
[62] J. Taler, B. Węglowski, D. Taler, M. Trojan, T. Sobota, P. Dzierwa, M. Pilarczyk, P. Madejski, D. Nabagło, Method of determination of thermowell parameters for steam boiler, Journal of Power Technologies 95 (4) (2015) 309–316.
[63] M. Feidt, Thermodynamics of energy systems and processes: A review and perspectives, J. Appl. Fluid Mech 5 (2) (2012) 85–98.